Supporting Information

Stacking Order Dependent Second Harmonic Generation and Topological Defects in *h*-BN Bilayers

Cheol-Joo Kim[†], Lola Brown[†], Matt W. Graham[‡,§], Robert Hovden[∥], Robin W. Havener[∥], Paul L. McEuen[‡,§], David A. Muller[§,∥] and Jiwoong Park[†,§,*]

[†]Department of Chemistry and Chemical Biology, Cornell University, Ithaca, NY 14853, USA
[‡]Laboratory for Atomic and Solid State Physics, Cornell University, Ithaca, NY 14853, USA
[§]Kavli Institute at Cornell for Nanoscale Science, Ithaca, NY 14853, USA
[∥]School of Applied and Engineering Physics, Cornell University, Ithaca, NY 14853, USA

[*]email: *jpark@cornell.edu*

1. Epitaxial growth of hexagonal boron nitride (*h*-BN)

h-BN are synthesized by catalytic chemical vapor deposition (CVD) on either 99.8 % pure copper foils (Alfa Aesar #13382) or sputtered copper films with a thickness of 700 nm on sapphire c-planes.[1,2] Substrates are annealed in 1000 ^{o}C for 30 min with 100 sccm of hydrogen before the growths, and gas phase precursors are injected at 1000 ^{o}C by sublimating ammonia borane, NH_3BH_3 (Sigma Aldrich, Product #: 682098) at 60-85 ^{o}C in a separate heating tube, connected to the inlet of the reaction chamber. Growth time is varied from 8 to 270 min to obtain different sample thicknesses. For multilayer *h*-BN, copper foils are used, instead of sputtered copper films.

Due to the epitaxial relationships between *h*-BN and copper surfaces, *h*-BN is aligned to certain orientations. Figure S1a and S1b show dark field transmission electron microscopy (DF-TEM) images of

sub monolayer *h*-BN samples grown on Cu (100), a copper foil and Cu (111), a sputtered copper film on a sapphire c-plane, respectively. While Fig. S1a shows two predominant six-fold crystal diffraction patterns with a 30° angle difference, Fig. S2b shows well aligned single crystalline structures. These epitaxial growths are consistent with previously reported epitaxial growth of *h*-BN on Cu (100) and Cu (111) surface, where *h*-BN lattice constant and copper atom to atom distance toward <110> directions are similar each other as 2.504 Å and 2.546 Å respectively.

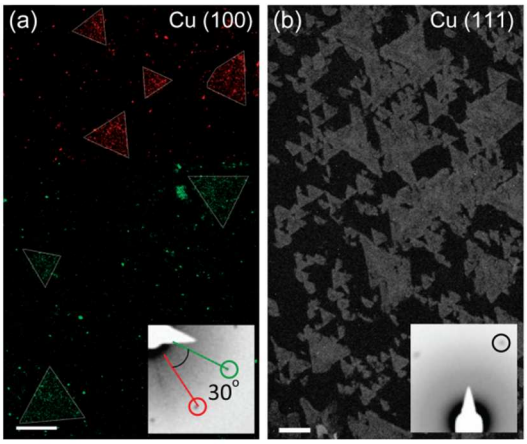

Figure S1 (a-b) DF-TEM images of *h*-BN sub monolayers grown on (a) Cu (100) and (b) Cu (111) surface. There are two predominant orientations of observed hexagonal diffraction patterns with a 30° angle difference in Fig. S1a, while they are all aligned to a certain direction in Fig. S1b. Scale bar are 200 nm and 2 μm for (a) and (b), respectively.

2. TEM characterization of *h*-BN stacking structures

For a TEM sample preparation, we follow a standard transfer method, described in elsewhere.[3] DF-TEM is conducted on an FEI Technai T12, operated at 60 kV, careful to remain below the energy threshold for the knock-on damage of boron and nitrogen atoms, which is 74 keV and 84 keV, respectively.[4]

In Fig. 2c and 2d of the main text, the intensities of DF-TEM images are determined by a phase difference between diffracted electron beams from each layer, which is highly sensitive to the lateral inter-layer translation. Therefore, the AA' stacking order, with no lateral translation, shows a constructive interference for both the inner diffraction spot, Φ_i and the outer diffraction spot, Φ_o. However, the AB stacking order s creates a phase difference, depending on the diffraction spot. For example, the Φ_i diffraction spot corresponds to the (0-110) crystal diffraction lattice planes with a lattice spacing of $3a/2$. As the top layer of AB bilayer is shifted by $a/2$ (or a) toward the [0-110] crystalline orientation, there is a large phase shift of 2π/3 (or 4π/3), resulting in the suppressed DF-TEM intensities

as seen at Fig. 2d. On the other hand, an outer diffraction spot, Φ_o, corresponds to (0-210) crystal diffraction lattice planes, with a lattice spacing of $\sqrt{3}a/2$, and there is no net phase difference in AB stacking order as the top layer is shifted by $\sqrt{3}a/2$ toward [0-210] direction. (see Fig. 2c in the main text)

Furthermore, we identify the atomic configurations by analyzing selected area electron diffraction (SAED) data as a function of a sample tilt angle with respect to an incident beam. Figure S2a depicts the schematics of the most stable atomic configurations for *h*-BN bilayers, AB and AA' structures, with the diffraction planes for Φ_i and Φ_o in each case. Figure S2b shows intensity plots for three diffraction spots observed in AB and AA' structures as a function of the sample tilt angle. Spot intensities are extracted from each area by using 6 parameter Gaussian fits after background subtraction to consider the changes in the gaussian width from surface variations. Experimental data is consistent with the theoretical curves for AB stacking and AA' stacking of bilayer *h*-BN.[5,6]

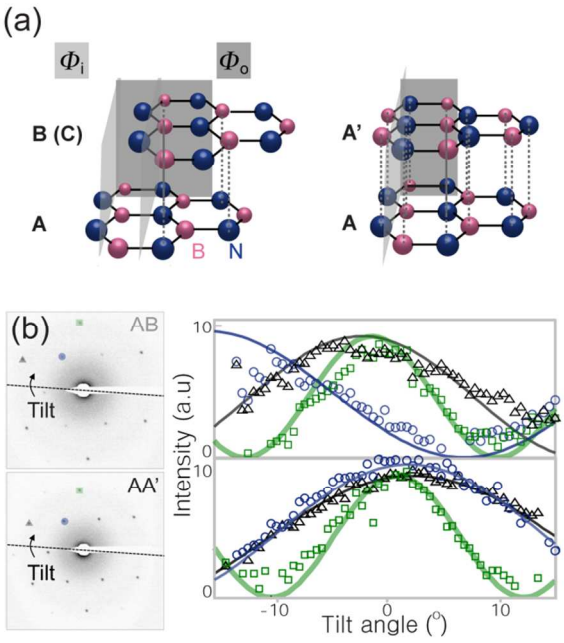

Figure S2 (a) Schematics of two structural ground states, AB and AA' stacking. Gray boxes indicate diffraction lattice planes for Φ_i and Φ_o of a diffraction pattern. (b) Diffraction patterns of AB and AA' stackings and intensity changes of three representative spots as a function of the sample tilt angle with respect to the incident beam. Solid lines are calculated from theoretical kinematic diffraction of a 60 keV electron beam.

We note that diffraction signals from some structural variations are very similar. Figure S3a shows three structures of AB, AB' and AC' *h*-BN bilayer. While they have a same graphitic stacking structure, only difference is the arrangement of constituting atoms; AB (boron on the top of nitrogen), AB' (boron on the top of boron) and AC' (nitrogen on the top of nitrogen). Figure S3b-c show theoretically predicted diffraction spot intensity as a function of the sample tilt angle with respect to the incident electron beam. Due to the slightly different scattering factors of boron and nitrogen in our measurement condition, they result in slight changes in the values and require careful measurements and data analyses including proper background corrections for structural identifications. To check the structures more clearly, we conduct correlated SHG measurements which indicated only AB structures without AB' and AC' structures.

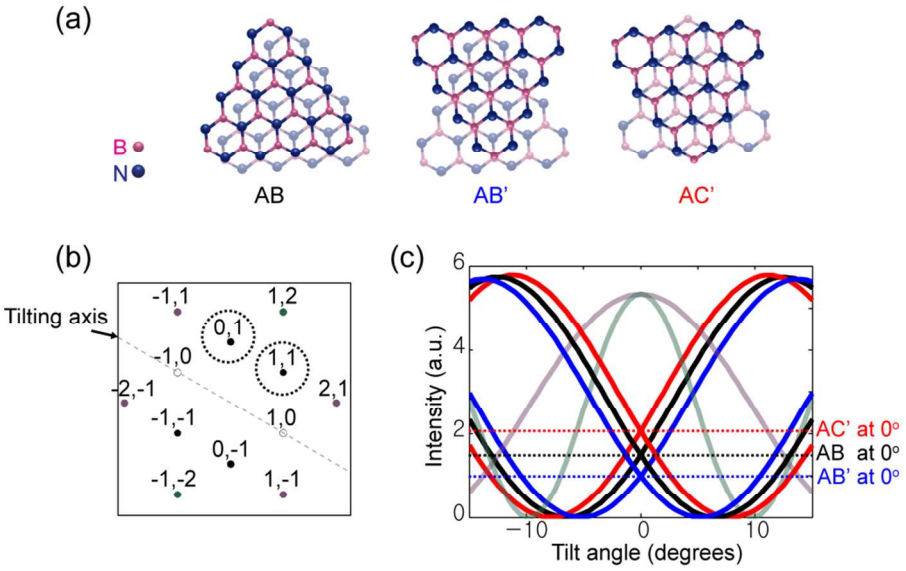

Figure S3 (a) Schematics of AB (boron on the top of nitrogen), AB' (boron on the top of boron) and AC' (nitrogen on the top of nitrogen) stacking structures (b) Color coded diffraction pattern with a tilt axis. (c) Calculated intensity changes of each diffraction spot as a function of the sample tilt angle for AB, AB' and AC' structures, assuming a flat Ewald sphere. Dotted lines indicate the intensities of (0,1) and (1,1) diffraction spots (circled by dotted lines in Fig. S3b) at a 0^{o} tilt angle for each structure, showing subtle differences.

3. Fitting of the width of topological defect lines

In the equation for indicating the width of topological defect lines (see the manuscript), lattice structure related constant, *A*, strain related constant, *B*, and mechanical modulus, *M* are denoted as

follow. $A = 4L/(3\sqrt{3}d^2)$, $B = T \cdot L/4$, where *L* is the length of dislocations, *d* is the carbon atom to atom distance, *T* is the total atomic transition length over the defect structures. $M = G + (Y/(1-\nu^2) - G)\cos^2\alpha$, where *G* is shear modulus, *Y* is young's modulus, ν is Poisson ratio, α is the relative angle between *T* and the vector normal to the defect lines. For fitting, reported *Y* of 256 GPa·nm and ν of 0.208 for *h*-BN crystal are substituted[7] and we deduce shear modulus of 26.4 GPa·nm as a free parameter.[7] Finally, U_0 of dislocations are estimated as 0.488 meV/atom and 3.03 meV/atom in AB (or AC) and AA' stacking structures, respectively, which are closely matched with theoretical values of 0.545 meV/atom for AB and 3.855 meV/atom for AA', closely.[8]

4. Second harmonic generation (SHG) measurement

For non-linear optical susceptibility, a radiation from a mode-locked Ti:sapphire oscillator, operating at 76 MHz repetition rate with 180 fs duration pulse is focused on the sample with an objective of N.A. of 0.6, being centered at a wavelength of 810 nm. We measure frequency doubled reflectance signal by a photomultiplier after passing consecutive band pass filters, centered at 405 nm with a FWHM of 15 nm. For polarization dependent measurement, polarization of injected light is rotating with respect to the sample and the polarization of emission light is set to be parallel with it.

Figure S4 shows a plot of the square root of SHG as a function of pulse fluence, showing an expected linear slope in two photon nonlinear processes. We note that SHG effect from amorphous film is negligible compared to the signal from *h*-BN crystal structures.

We estimate that the SHG intensity measured from our *h*-BN sample is significantly weaker (by a factor larger than 10) than that measured from a type I β-BaB_2O_4 crystal (theta = 22.8^o). Previously, it was reported that this β-BaB_2O_4 crystal and exfoliated *h*-BN crystals show comparable SHG intensities.[9] While this suggests that the SHG intensities are affected by the sample quality and thus can be used to investigate the quality of CVD grown samples, more systematic study is required in order to establish a quantitative relationship.

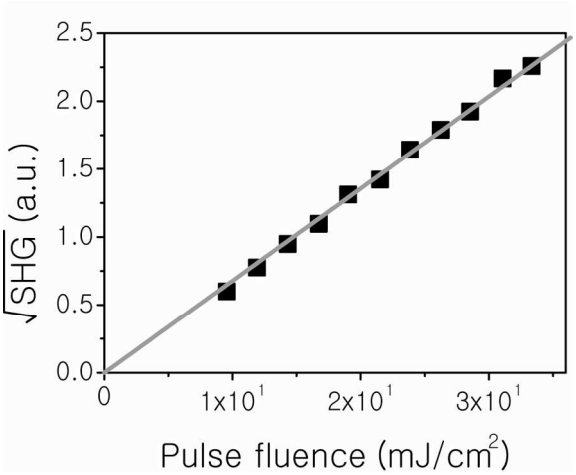

Figure S4 Incident pulse fluence dependence on the square root of SHG in *h*-BN AB stacking structures.

References

(1) Song, L.; Ci, L.; Lu, H.; Sorokin, P. B.; Jin, C.; Ni, J.; Kvashnin, A. G.; Kvashnin, D. G.; Lou, J.; Yakobson, B. I.; Ajayan, P. M. *Nano Letters* **2010**, *10*, 3209–3215.

(2) Kim, K. K.; Hsu, A.; Jia, X.; Kim, S. M.; Shi, Y.; Hofmann, M.; Nezich, D.; Rodriguez-Nieva, J. F.; Dresselhaus, M.; Palacios, T.; Kong, J. *Nano Letters* **2011**, *12*, 161-166.

(3) Huang, P. Y.; Ruiz-Vargas, C. S.; Van der Zande, A. M.; Whitney, W. S.; Levendorf, M. P.; Kevek, J. W.; Garg, S.; Alden, J. S.; Hustedt, C. J.; Zhu, Y.; Park, J.; McEuen, P. L.; Muller, D. A. *Nature* **2011**, *469*, 389–392.

(4) Alem, N.; Erni, R.; Kisielowski, C.; Rossell, M.; Gannett, W.; Zettl, A. *Physical Review B* **2009**, *80*, 1–7.

(5) Brown, L.; Hovden, R.; Huang, P.; Wojcik, M.; Muller, D. A; Park, J. *Nano Letters* **2012**, *12*, 1609–1615.

(6) Meyer, J. C.; Geim, A. K.; Katsnelson, M. I.; Novoselov, K. S.; Booth, T. J.; Roth, S. *Nature* **2007**, *446*, 60–63.

(7) Boldrin, L.; Scarpa, F.; Chowdhury, R.; Adhikari, S. *Nanotechnology* **2011**, *22*, 505702.

(8) Constantinescu, G.; Kuc, A.; Heine, T. *Physical Review Letters* **2013**, *111*, 036104.

(9) Li, Y.; Rao, Y.; Mak, K. F.; You, Y.; Wang, S.; Dean, C. R.; Heinz, T. F. *Nano Letters* **2013**, *13*, 3329-3333.